

Precise Measurement of Born Cross Sections for $e^+e^- \rightarrow D\bar{D}$ and Observation of One Structure between $\sqrt{s} = 3.80 - 4.95$ GeV

- M. Ablikim¹, M. N. Achasov^{5,b}, P. Adlarson⁷⁵, X. C. Ai⁸¹, R. Aliberti³⁶, A. Amoroso^{74A,74C}, M. R. An⁴⁰, Q. An^{71,58}, Y. Bai⁵⁷, O. Bakina³⁷, I. Balossino^{30A}, Y. Ban^{47,g}, V. Batozskaya^{1,45}, K. Begzsuren³³, N. Berger³⁶, M. Berlowski⁴⁵, M. Bertani^{29A}, D. Bettone^{30A}, F. Bianchi^{74A,74C}, E. Bianco^{74A,74C}, A. Bortone^{74A,74C}, I. Boyko³⁷, R. A. Briere⁶, A. Brueggemann⁶⁸, H. Cai⁷⁶, X. Cai^{1,58}, A. Calcaterra^{29A}, G. F. Cao^{1,63}, N. Cao^{1,63}, S. A. Cetin^{62A}, J. F. Chang^{1,58}, T. T. Chang⁷⁷, W. L. Chang^{1,63}, G. R. Che⁴⁴, G. Chelkov^{37,a}, C. Chen⁴⁴, Chao Chen⁵⁵, G. Chen¹, H. S. Chen^{1,63}, M. L. Chen^{1,58,63}, S. J. Chen⁴³, S. L. Chen⁴⁶, S. M. Chen⁶¹, T. Chen^{1,63}, X. R. Chen^{32,63}, X. T. Chen^{1,63}, Y. B. Chen^{1,58}, Y. Q. Chen³⁵, Z. J. Chen^{26,h}, W. S. Cheng^{74C}, S. K. Choi^{11A}, X. Chu⁴⁴, G. Cibinetto^{30A}, S. C. Coen⁴, F. Cossio^{74C}, J. J. Cui⁵⁰, H. L. Dai^{1,58}, J. P. Dai⁷⁹, A. Dbeysi¹⁹, R. E. de Boer⁴, D. Dedovich³⁷, Z. Y. Deng¹, A. Denig³⁶, I. Denysenko³⁷, M. Destefanis^{74A,74C}, F. De Mori^{74A,74C}, B. Ding^{66,1}, X. X. Ding^{47,g}, Y. Ding³⁵, Y. Ding⁴¹, J. Dong^{1,58}, L. Y. Dong^{1,63}, M. Y. Dong^{1,58,63}, X. Dong⁷⁶, M. C. Du¹, S. X. Du⁸¹, Z. H. Duan⁴³, P. Egorov^{37,a}, Y. H. Fan⁴⁶, J. Fang^{1,58}, S. S. Fang^{1,63}, W. X. Fang¹, Y. Fang¹, R. Farinelli^{30A}, L. Fava^{74B,74C}, F. Feldbauer⁴, G. Felici^{29A}, C. Q. Feng^{71,58}, J. H. Feng⁵⁹, K. Fischer⁶⁹, M. Fritsch⁴, C. D. Fu¹, J. L. Fu⁶³, Y. W. Fu¹, H. Gao⁶³, Y. N. Gao^{47,g}, Yang Gao^{71,58}, S. Garbolino^{74C}, I. Garzia^{30A,30B}, P. T. Ge⁷⁶, Z. W. Ge⁴³, C. Geng⁵⁹, E. M. Gersabeck⁶⁷, A. Gilman⁶⁹, K. Goetzen¹⁴, L. Gong⁴¹, W. X. Gong^{1,58}, W. Gradl³⁶, S. Gramigna^{30A,30B}, M. Greco^{74A,74C}, M. H. Gu^{1,58}, Y. T. Gu¹⁶, C. Y. Guan^{1,63}, Z. L. Guan²³, A. Q. Guo^{32,63}, L. B. Guo⁴², M. J. Guo⁵⁰, R. P. Guo⁴⁹, Y. P. Guo^{13,f}, A. Guskov^{37,a}, T. T. Han⁵⁰, W. Y. Han⁴⁰, X. Q. Hao²⁰, F. A. Harris⁶⁵, K. K. He⁵⁵, K. L. He^{1,63}, F. H. H.. Heinsius⁴, C. H. Heinz³⁶, Y. K. Heng^{1,58,63}, C. Herold⁶⁰, T. Holtmann⁴, P. C. Hong^{13,f}, G. Y. Hou^{1,63}, X. T. Hou^{1,63}, Y. R. Hou⁶³, Z. L. Hou¹, H. M. Hu^{1,63}, J. F. Hu^{56,i}, T. Hu^{1,58,63}, Y. Hu¹, G. S. Huang^{71,58}, K. X. Huang⁵⁹, L. Q. Huang^{32,63}, X. T. Huang⁵⁰, Y. P. Huang¹, T. Hussain⁷³, N. in der Wiesche⁶⁸, M. Irshad^{71,58}, J. Jackson²⁸, S. Jaeger⁴, S. Janchiv³³, J. H. Jeong^{11A}, Q. Ji¹, Q. P. Ji²⁰, X. B. Ji^{1,63}, X. L. Ji^{1,58}, Y. Y. Ji⁵⁰, X. Q. Jia⁵⁰, Z. K. Jia^{71,58}, H. J. Jiang⁷⁶, P. C. Jiang^{47,g}, S. S. Jiang⁴⁰, T. J. Jiang¹⁷, X. S. Jiang^{1,58,63}, Y. Jiang⁶³, J. B. Jiao⁵⁰, Z. Jiao²⁴, S. Jin⁴³, Y. Jin⁶⁶, M. Q. Jing^{1,63}, T. Johansson⁷⁵, X. K.¹, S. Kabana³⁴, N. Kalantar-Nayestanaki⁶⁴, X. L. Kang¹⁰, X. S. Kang⁴¹, M. Kavatsyuk⁶⁴, B. C. Ke⁸¹, A. Khoukaz⁶⁸, R. Kiuchi¹, R. Kliemt¹⁴, O. B. Kolcu^{62A}, B. Kopf⁴, M. Kuessner⁴, A. Kupsc^{45,75}, W. Kühn³⁸, J. J. Lane⁶⁷, P. Larin¹⁹, A. Lavania²⁷, L. Lavezzi^{74A,74C}, T. T. Lei^{71,58}, Z. H. Lei^{71,58}, H. Leithoff³⁶, M. Lellmann³⁶, T. Lenz³⁶, C. Li⁴⁴, C. Li⁴⁸, C. H. Li⁴⁰, Cheng Li^{71,58}, D. M. Li⁸¹, F. Li^{1,58}, G. Li¹, H. Li^{71,58}, H. B. Li^{1,63}, H. J. Li²⁰, H. N. Li^{56,i}, Hui Li⁴⁴, J. R. Li⁶¹, J. S. Li⁵⁹, J. W. Li⁵⁰, K. L. Li²⁰, Ke Li¹, L. J. Li^{1,63}, L. K. Li¹, Lei Li³, M. H. Li⁴⁴, P. R. Li^{39,j,k}, Q. X. Li⁵⁰, S. X. Li¹³, T. Li⁵⁰, W. D. Li^{1,63}, W. G. Li¹, X. H. Li^{71,58}, X. L. Li⁵⁰, Xiaoyu Li^{1,63}, Y. G. Li^{47,g}, Z. J. Li⁵⁹, Z. X. Li¹⁶, C. Liang⁴³, H. Liang^{1,63}, H. Liang³⁵, H. Liang^{71,58}, Y. F. Liang⁵⁴, Y. T. Liang^{32,63}, G. R. Liao¹⁵, L. Z. Liao⁵⁰, Y. P. Liao^{1,63}, J. Libby²⁷, A. Limphirat⁶⁰, D. X. Lin^{32,63}, T. Lin¹, B. J. Liu¹, B. X. Liu⁷⁶, C. Liu³⁵, C. X. Liu¹, F. H. Liu⁵³, Fang Liu¹, Feng Liu⁷, G. M. Liu^{56,i}, H. Liu^{39,j,k}, H. B. Liu¹⁶, H. M. Liu^{1,63}, Huanhuan Liu¹, Huihui Liu²², J. B. Liu^{71,58}, J. L. Liu⁷², J. Y. Liu^{1,63}, K. Liu¹, K. Y. Liu⁴¹, Ke Liu²³, L. Liu^{71,58}, L. C. Liu⁴⁴, Lu Liu⁴⁴, M. H. Liu^{13,f}, P. L. Liu¹, Q. Liu⁶³, S. B. Liu^{71,58}, T. Liu^{13,f}, W. K. Liu⁴⁴, W. M. Liu^{71,58}, X. Liu^{39,j,k}, Y. Liu⁸¹, Y. B. Liu⁴⁴, Z. A. Liu^{1,58,63}, Z. Q. Liu⁵⁰, X. C. Lou^{1,58,63}, F. X. Lu⁵⁹, H. J. Lu²⁴, J. G. Lu^{1,58}, X. L. Lu¹, Y. Lu⁸, Y. P. Lu^{1,58}, Z. H. Lu^{1,63}, C. L. Luo⁴², M. X. Luo⁸⁰, T. Luo^{13,f}, X. L. Luo^{1,58}, X. R. Lyu⁶³, Y. F. Lyu⁴⁴, F. C. Ma⁴¹, H. L. Ma¹, J. L. Ma^{1,63}, L. L. Ma⁵⁰, M. M. Ma^{1,63}, Q. M. Ma¹, R. Q. Ma^{1,63}, R. T. Ma⁶³, X. Y. Ma^{1,58}, Y. Ma^{47,g}, Y. M. Ma³², F. E. Maas¹⁹, M. Maggiore^{74A,74C}, S. Malde⁶⁹, Q. A. Malik⁷³, A. Mangoni^{29B}, Y. J. Mao^{47,g}, Z. P. Mao¹, S. Marcello^{74A,74C}, Z. X. Meng⁶⁶, J. G. Messchendorp^{14,64}, G. Mezzadri^{30A}, H. Miao^{1,63}, T. J. Min⁴³, R. E. Mitchell²⁸, X. H. Mo^{1,58,63}, N. Yu. Muchnoi^{5,b}, J. Muskalla³⁶, Y. Nefedov³⁷, F. Nerling^{19,d}, I. B. Nikolaev^{5,b}, Z. Ning^{1,58}, S. Nisar^{12,l}, Q. L. Niu^{39,j,k}, W. D. Niu⁵⁵, Y. Niu⁵⁰, S. L. Olsen⁶³, Q. Ouyang^{1,58,63}, S. Pacetti^{29B,29C}, X. Pan⁵⁵, Y. Pan⁵⁷, A. Pathak³⁵, P. Patteri^{29A}, Y. P. Pei^{71,58}, M. Pelizaeus⁴, H. P. Peng^{71,58}, Y. Y. Peng^{39,j,k}, K. Peters^{14,d}, J. L. Ping⁴², R. G. Ping^{1,63}, S. Plura³⁶, V. Prasad³⁴, F. Z. Qi¹, H. Qi^{71,58}, H. R. Qi⁶¹, M. Qi⁴³, T. Y. Qi^{13,f}, S. Qian^{1,58}, W. B. Qian⁶³, C. F. Qiao⁶³, J. J. Qin⁷², L. Q. Qin¹⁵, X. P. Qin^{13,f}, X. S. Qin⁵⁰, Z. H. Qin^{1,58}, J. F. Qiu¹, S. Q. Qu⁶¹, C. F. Redmer³⁶, K. J. Ren⁴⁰, A. Rivetti^{74C}, M. Rolo^{74C}, G. Rong^{1,63}, Ch. Rosner¹⁹, S. N. Ruan⁴⁴, N. Salone⁴⁵, A. Sarantsev^{37,c}, Y. Schelhaas³⁶, K. Schoenning⁷⁵, M. Scodeggio^{30A,30B}, K. Y. Shan^{13,f}, W. Shan²⁵, X. Y. Shan^{71,58}, J. F. Shangguan⁵⁵, L. G. Shao^{1,63}, M. Shao^{71,58}, C. P. Shen^{13,f}, H. F. Shen^{1,63}, W. H. Shen⁶³, X. Y. Shen^{1,63}, B. A. Shi⁶³, H. C. Shi^{71,58}, J. L. Shi¹³, J. Y. Shi¹, Q. Q. Shi⁵⁵, R. S. Shi^{1,63}, X. Shi^{1,58}, J. J. Song²⁰, T. Z. Song⁵⁹, W. M. Song^{35,1}, Y. J. Song¹³, Y. X. Song^{47,g}, S. Sosio^{74A,74C}, S. Spataro^{74A,74C}, F. Stieler³⁶, Y. J. Su⁶³, G. B. Sun⁷⁶, G. X. Sun¹, H. Sun⁶³, H. K. Sun¹, J. F. Sun²⁰, K. Sun⁶¹, L. Sun⁷⁶, S. S. Sun^{1,63}, T. Sun^{1,63}, W. Y. Sun³⁵, Y. Sun¹⁰, Y. J. Sun^{71,58}, Y. Z. Sun¹, Z. T. Sun⁵⁰, Y. X. Tan^{71,58}, C. J. Tang⁵⁴, G. Y. Tang¹, J. Tang⁵⁹, Y. A. Tang⁷⁶, L. Y. Tao⁷², Q. T. Tao^{26,h}, M. Tat⁶⁹, J. X. Teng^{71,58}, V. Thoren⁷⁵, W. H. Tian⁵⁹,

W. H. Tian⁵², Y. Tian^{32,63}, Z. F. Tian⁷⁶, I. Uman^{62B}, S. J. Wang⁵⁰, B. Wang¹, B. L. Wang⁶³, Bo Wang^{71,58}, C. W. Wang⁴³, D. Y. Wang^{47,g}, F. Wang⁷², H. J. Wang^{39,j,k}, H. P. Wang^{1,63}, J. P. Wang⁵⁰, K. Wang^{1,58}, L. L. Wang¹, M. Wang⁵⁰, Meng Wang^{1,63}, S. Wang^{13,f}, S. Wang^{39,j,k}, T. Wang^{13,f}, T. J. Wang⁴⁴, W. Wang⁷², W. Wang⁵⁹, W. P. Wang^{71,58}, X. Wang^{47,g}, X. F. Wang^{39,j,k}, X. J. Wang⁴⁰, X. L. Wang^{13,f}, Y. Wang⁶¹, Y. D. Wang⁴⁶, Y. F. Wang^{1,58,63}, Y. H. Wang⁴⁸, Y. N. Wang⁴⁶, Y. Q. Wang¹, Yaqian Wang^{18,1}, Yi Wang⁶¹, Z. Wang^{1,58}, Z. L. Wang⁷², Z. Y. Wang^{1,63}, Ziyi Wang⁶³, D. Wei⁷⁰, D. H. Wei¹⁵, F. Weidner⁶⁸, S. P. Wen¹, C. W. Wenzel⁴, U. Wiedner⁴, G. Wilkinson⁶⁹, M. Wolke⁷⁵, L. Wollenberg⁴, C. Wu⁴⁰, J. F. Wu^{1,63}, L. H. Wu¹, L. J. Wu^{1,63}, X. Wu^{13,f}, X. H. Wu³⁵, Y. Wu⁷¹, Y. H. Wu⁵⁵, Y. J. Wu³², Z. Wu^{1,58}, L. Xia^{71,58}, X. M. Xian⁴⁰, T. Xiang^{47,g}, D. Xiao^{39,j,k}, G. Y. Xiao⁴³, S. Y. Xiao¹, Y. L. Xiao^{13,f}, Z. J. Xiao⁴², C. Xie⁴³, X. H. Xie^{47,g}, Y. Xie⁵⁰, Y. G. Xie^{1,58}, Y. H. Xie⁷, Z. P. Xie^{71,58}, T. Y. Xing^{1,63}, C. F. Xu^{1,63}, C. J. Xu⁵⁹, G. F. Xu¹, H. Y. Xu⁶⁶, Q. J. Xu¹⁷, Q. N. Xu³¹, W. Xu^{1,63}, W. L. Xu⁶⁶, X. P. Xu⁵⁵, Y. C. Xu⁷⁸, Z. P. Xu⁴³, Z. S. Xu⁶³, F. Yan^{13,f}, L. Yan^{13,f}, W. B. Yan^{71,58}, W. C. Yan⁸¹, X. Q. Yan¹, H. J. Yang^{51,e}, H. L. Yang³⁵, H. X. Yang¹, Tao Yang¹, Y. Yang^{13,f}, Y. F. Yang⁴⁴, Y. X. Yang^{1,63}, Yifan Yang^{1,63}, Z. W. Yang^{39,j,k}, Z. P. Yao⁵⁰, M. Ye^{1,58}, M. H. Ye⁹, J. H. Yin¹, Z. Y. You⁵⁹, B. X. Yu^{1,58,63}, C. X. Yu⁴⁴, G. Yu^{1,63}, J. S. Yu^{26,h}, T. Yu⁷², X. D. Yu^{47,g}, C. Z. Yuan^{1,63}, L. Yuan², S. C. Yuan¹, X. Q. Yuan¹, Y. Yuan^{1,63}, Z. Y. Yuan⁵⁹, C. X. Yue⁴⁰, A. A. Zafar⁷³, F. R. Zeng⁵⁰, X. Zeng^{13,f}, Y. Zeng^{26,h}, Y. J. Zeng^{1,63}, X. Y. Zhai³⁵, Y. C. Zhai⁵⁰, Y. H. Zhan⁵⁹, A. Q. Zhang^{1,63}, B. L. Zhang^{1,63}, B. X. Zhang¹, D. H. Zhang⁴⁴, G. Y. Zhang²⁰, H. Zhang⁷¹, H. C. Zhang^{1,58,63}, H. H. Zhang⁵⁹, H. H. Zhang³⁵, H. Q. Zhang^{1,58,63}, H. Y. Zhang^{1,58}, J. Zhang⁸¹, J. J. Zhang⁵², J. L. Zhang²¹, J. Q. Zhang⁴², J. W. Zhang^{1,58,63}, J. X. Zhang^{39,j,k}, J. Y. Zhang¹, J. Z. Zhang^{1,63}, Jianyu Zhang⁶³, Jiawei Zhang^{1,63}, L. M. Zhang⁶¹, L. Q. Zhang⁵⁹, Lei Zhang⁴³, P. Zhang^{1,63}, Q. Y. Zhang^{40,81}, Shuihan Zhang^{1,63}, Shulei Zhang^{26,h}, X. D. Zhang⁴⁶, X. M. Zhang¹, X. Y. Zhang⁵⁰, Xuyan Zhang⁵⁵, Y. Zhang⁶⁹, Y. Zhang⁷², Y. T. Zhang⁸¹, Y. H. Zhang^{1,58}, Yan Zhang^{71,58}, Yao Zhang¹, Z. H. Zhang¹, Z. L. Zhang³⁵, Z. Y. Zhang⁴⁴, Z. Y. Zhang⁷⁶, G. Zhao¹, J. Zhao⁴⁰, J. Y. Zhao^{1,63}, J. Z. Zhao^{1,58}, Lei Zhao^{71,58}, Ling Zhao¹, M. G. Zhao⁴⁴, S. J. Zhao⁸¹, Y. B. Zhao^{1,58}, Y. X. Zhao^{32,63}, Z. G. Zhao^{71,58}, A. Zhemchugov^{37,a}, B. Zheng⁷², J. P. Zheng^{1,58}, W. J. Zheng^{1,63}, Y. H. Zheng⁶³, B. Zhong⁴², X. Zhong⁵⁹, H. Zhou⁵⁰, L. P. Zhou^{1,63}, X. Zhou⁷⁶, X. K. Zhou⁷, X. R. Zhou^{71,58}, X. Y. Zhou⁴⁰, Y. Z. Zhou^{13,f}, J. Zhu⁴⁴, K. Zhu¹, K. J. Zhu^{1,58,63}, L. Zhu³⁵, L. X. Zhu⁶³, S. H. Zhu⁷⁰, S. Q. Zhu⁴³, T. J. Zhu^{13,f}, W. J. Zhu^{13,f}, Y. C. Zhu^{71,58}, Z. A. Zhu^{1,63}, J. H. Zou¹, J. Zu^{71,58}

(BESIII Collaboration)

¹ Institute of High Energy Physics, Beijing 100049, People's Republic of China

² Beihang University, Beijing 100191, People's Republic of China

³ Beijing Institute of Petrochemical Technology, Beijing 102617, People's Republic of China

⁴ Bochum Ruhr-University, D-44780 Bochum, Germany

⁵ Budker Institute of Nuclear Physics SB RAS (BINP), Novosibirsk 630090, Russia

⁶ Carnegie Mellon University, Pittsburgh, Pennsylvania 15213, USA

⁷ Central China Normal University, Wuhan 430079, People's Republic of China

⁸ Central South University, Changsha 410083, People's Republic of China

⁹ China Center of Advanced Science and Technology, Beijing 100190, People's Republic of China

¹⁰ China University of Geosciences, Wuhan 430074, People's Republic of China

¹¹ Chung-Ang University, Seoul, 06974, Republic of Korea

¹² COMSATS University Islamabad, Lahore Campus, Defence Road, Off Raiwind Road, 54000 Lahore, Pakistan

¹³ Fudan University, Shanghai 200433, People's Republic of China

¹⁴ GSI Helmholtzcentre for Heavy Ion Research GmbH, D-64291 Darmstadt, Germany

¹⁵ Guangxi Normal University, Guilin 541004, People's Republic of China

¹⁶ Guangxi University, Nanning 530004, People's Republic of China

¹⁷ Hangzhou Normal University, Hangzhou 310036, People's Republic of China

¹⁸ Hebei University, Baoding 071002, People's Republic of China

¹⁹ Helmholtz Institute Mainz, Staudinger Weg 18, D-55099 Mainz, Germany

²⁰ Henan Normal University, Xinxiang 453007, People's Republic of China

²¹ Henan University, Kaifeng 475004, People's Republic of China

²² Henan University of Science and Technology, Luoyang 471003, People's Republic of China

²³ Henan University of Technology, Zhengzhou 450001, People's Republic of China

²⁴ Huangshan College, Huangshan 245000, People's Republic of China

²⁵ Hunan Normal University, Changsha 410081, People's Republic of China

²⁶ Hunan University, Changsha 410082, People's Republic of China

- ²⁷ Indian Institute of Technology Madras, Chennai 600036, India
²⁸ Indiana University, Bloomington, Indiana 47405, USA
- ²⁹ INFN Laboratori Nazionali di Frascati , (A)INFN Laboratori Nazionali di Frascati, I-00044, Frascati, Italy; (B)INFN Sezione di Perugia, I-06100, Perugia, Italy; (C)University of Perugia, I-06100, Perugia, Italy
- ³⁰ INFN Sezione di Ferrara, (A)INFN Sezione di Ferrara, I-44122, Ferrara, Italy; (B)University of Ferrara, I-44122, Ferrara, Italy
- ³¹ Inner Mongolia University, Hohhot 010021, People's Republic of China
- ³² Institute of Modern Physics, Lanzhou 730000, People's Republic of China
- ³³ Institute of Physics and Technology, Peace Avenue 54B, Ulaanbaatar 13330, Mongolia
- ³⁴ Instituto de Alta Investigación, Universidad de Tarapacá, Casilla 7D, Arica 1000000, Chile
- ³⁵ Jilin University, Changchun 130012, People's Republic of China
- ³⁶ Johannes Gutenberg University of Mainz, Johann-Joachim-Becher-Weg 45, D-55099 Mainz, Germany
- ³⁷ Joint Institute for Nuclear Research, 141980 Dubna, Moscow region, Russia
- ³⁸ Justus-Liebig-Universitaet Giessen, II. Physikalisches Institut, Heinrich-Buff-Ring 16, D-35392 Giessen, Germany
- ³⁹ Lanzhou University, Lanzhou 730000, People's Republic of China
- ⁴⁰ Liaoning Normal University, Dalian 116029, People's Republic of China
- ⁴¹ Liaoning University, Shenyang 110036, People's Republic of China
- ⁴² Nanjing Normal University, Nanjing 210023, People's Republic of China
- ⁴³ Nanjing University, Nanjing 210093, People's Republic of China
- ⁴⁴ Nankai University, Tianjin 300071, People's Republic of China
- ⁴⁵ National Centre for Nuclear Research, Warsaw 02-093, Poland
- ⁴⁶ North China Electric Power University, Beijing 102206, People's Republic of China
- ⁴⁷ Peking University, Beijing 100871, People's Republic of China
- ⁴⁸ Qufu Normal University, Qufu 273165, People's Republic of China
- ⁴⁹ Shandong Normal University, Jinan 250014, People's Republic of China
- ⁵⁰ Shandong University, Jinan 250100, People's Republic of China
- ⁵¹ Shanghai Jiao Tong University, Shanghai 200240, People's Republic of China
- ⁵² Shanxi Normal University, Linfen 041004, People's Republic of China
- ⁵³ Shanxi University, Taiyuan 030006, People's Republic of China
- ⁵⁴ Sichuan University, Chengdu 610064, People's Republic of China
- ⁵⁵ Soochow University, Suzhou 215006, People's Republic of China
- ⁵⁶ South China Normal University, Guangzhou 510006, People's Republic of China
- ⁵⁷ Southeast University, Nanjing 211100, People's Republic of China
- ⁵⁸ State Key Laboratory of Particle Detection and Electronics, Beijing 100049, Hefei 230026, People's Republic of China
- ⁵⁹ Sun Yat-Sen University, Guangzhou 510275, People's Republic of China
- ⁶⁰ Suranaree University of Technology, University Avenue 111, Nakhon Ratchasima 30000, Thailand
- ⁶¹ Tsinghua University, Beijing 100084, People's Republic of China
- ⁶² Turkish Accelerator Center Particle Factory Group, (A)Istinye University, 34010, Istanbul, Turkey; (B)Near East University, Nicosia, North Cyprus, 99138, Mersin 10, Turkey
- ⁶³ University of Chinese Academy of Sciences, Beijing 100049, People's Republic of China
- ⁶⁴ University of Groningen, NL-9747 AA Groningen, The Netherlands
- ⁶⁵ University of Hawaii, Honolulu, Hawaii 96822, USA
- ⁶⁶ University of Jinan, Jinan 250022, People's Republic of China
- ⁶⁷ University of Manchester, Oxford Road, Manchester, M13 9PL, United Kingdom
- ⁶⁸ University of Muenster, Wilhelm-Klemm-Strasse 9, 48149 Muenster, Germany
- ⁶⁹ University of Oxford, Keble Road, Oxford OX13RH, United Kingdom
- ⁷⁰ University of Science and Technology Liaoning, Anshan 114051, People's Republic of China
- ⁷¹ University of Science and Technology of China, Hefei 230026, People's Republic of China
- ⁷² University of South China, Hengyang 421001, People's Republic of China
- ⁷³ University of the Punjab, Lahore-54590, Pakistan
- ⁷⁴ University of Turin and INFN, (A)University of Turin, I-10125, Turin, Italy; (B)University

of Eastern Piedmont, I-15121, Alessandria, Italy; (C)INFN, I-10125, Turin, Italy

⁷⁵ *Uppsala University, Box 516, SE-75120 Uppsala, Sweden*

⁷⁶ *Wuhan University, Wuhan 430072, People's Republic of China*

⁷⁷ *Xinyang Normal University, Xinyang 464000, People's Republic of China*

⁷⁸ *Yantai University, Yantai 264005, People's Republic of China*

⁷⁹ *Yunnan University, Kunming 650500, People's Republic of China*

⁸⁰ *Zhejiang University, Hangzhou 310027, People's Republic of China*

⁸¹ *Zhengzhou University, Zhengzhou 450001, People's Republic of China*

^a *Also at the Moscow Institute of Physics and Technology, Moscow 141700, Russia*

^b *Also at the Novosibirsk State University, Novosibirsk, 630090, Russia*

^c *Also at the NRC "Kurchatov Institute", PNPI, 188300, Gatchina, Russia*

^d *Also at Goethe University Frankfurt, 60323 Frankfurt am Main, Germany*

^e *Also at Key Laboratory for Particle Physics, Astrophysics and Cosmology, Ministry of Education; Shanghai Key Laboratory for Particle Physics and Cosmology; Institute of Nuclear and Particle Physics, Shanghai 200240, People's Republic of China*

^f *Also at Key Laboratory of Nuclear Physics and Ion-beam Application (MOE) and Institute of Modern Physics, Fudan University, Shanghai 200443, People's Republic of China*

^g *Also at State Key Laboratory of Nuclear Physics and Technology, Peking University, Beijing 100871, People's Republic of China*

^h *Also at School of Physics and Electronics, Hunan University, Changsha 410082, China*

ⁱ *Also at Guangdong Provincial Key Laboratory of Nuclear Science, Institute of Quantum Matter, South China Normal University, Guangzhou 510006, China*

^j *Also at Frontiers Science Center for Rare Isotopes, Lanzhou University, Lanzhou 730000, People's Republic of China*

^k *Also at Lanzhou Center for Theoretical Physics, Key Laboratory of Theoretical Physics of Gansu Province, and Key Laboratory for Quantum Theory and Applications of MoE, Lanzhou University, Lanzhou 730000, People's Republic of China*

^l *Also at the Department of Mathematical Sciences, IBA, Karachi 75270, Pakistan*

(Dated: February 7, 2024)

Using data samples collected with the BESIII detector at the BEPCII collider at center-of-mass energies ranging from 3.80 to 4.95 GeV, corresponding to an integrated luminosity of 20 fb^{-1} , a measurement of Born cross sections for the $e^+e^- \rightarrow D^0\bar{D}^0$ and $D^+\bar{D}^-$ processes is presented with unprecedented precision. By performing a simultaneous fit to the dressed cross sections for both processes, one possible new structure around $3.9 \text{ GeV}/c^2$ is observed for the first time, in addition to seven known resonances $\psi(3770)$, $\psi(4040)$, $\psi(4160)$, $Y(4230)$, $Y(4360)$, $\psi(4415)$, and $Y(4660)$. These results offer crucial experimental insights into the nature of hadron production in the open charm region.

The production of hadrons in e^+e^- annihilation above the open-charm threshold is a topic of ongoing theoretical and experimental research. In 1980, a theoretical calculation for the charm cross section in e^+e^- annihilation was first attempted based on a coupled-channel potential model [1]. This calculation presented a prediction of the ΔR value ($\Delta R = \sum_i R_i$, where R_i stands for the ratio of individual hadron cross section to muon cross section in electron-positron collisions, i runs over the two-body channels) with the $D\bar{D}$ final states. According to this prediction, there are five vector charmonium states between 3.773 GeV ($\psi(3773)$, 1D state) and 4.95 GeV, namely, the $3S$, $2D$, $4S$, $3D$, and $5S$ states, dominated by the $D\bar{D}$ final states. In experimental studies, besides the three well-established structures observed in the inclusive hadronic cross sections [2], *i.e.*, $\psi(4040)$, $\psi(4160)$, and $\psi(4415)$, many new states, such as, $Y(4230)$, $Y(4260)$, $Y(4360)$ and $Y(4660)$, have been reported in the initial state radiation (ISR) processes at the B factories [3–11], or in the direct e^+e^- production at the CLEO [12] and BESIII exper-

iments [13–17]. Among them, the BESIII experiment found that the mass of $Y(4360)$ is around $4.3 \text{ GeV}/c^2$ [14], which is different from the value given by the Particle Data Group (PDG) [2]. The overpopulation of structures in this region and the mismatch of the properties between the potential model predictions and experimental measurements have led to various interpretations, such as hybrid states, tetraquark states, or molecular states [18, 19]. Although this information enriches our understanding of these exotic structures, the nature of these states is still not understood.

The studies of charmed meson pairs in e^+e^- annihilation above the open-charm threshold are expected to clarify the current understanding of these states. At present, the available observed cross sections of the $e^+e^- \rightarrow D\bar{D}$ process with limited energy points have been reported by B factories [20, 21] using the ISR process and through direct e^+e^- production at the CLEO experiment [22]. A precise measurement, particularly of the exclusive Born cross sections for $e^+e^- \rightarrow D\bar{D}$,

is highly desirable to validate the interpretations of the established states and provide insight into the energy region above the open-charm threshold.

In this Letter, we report a precise measurement of Born cross sections for the $e^+e^- \rightarrow D^0\bar{D}^0$ and $e^+e^- \rightarrow D^+D^-$ processes, specifically, at 150 center-of-mass (CM) energy points. Through a simultaneous fit to the dressed cross sections of both modes, eight resonances are observed, revealing seven known resonance structures and one possible new structure. Furthermore, the products of branching fractions and electronic partial widths for all assumed resonance structures are determined. The data sets used in this work correspond to a total luminosity of approximately 20 fb^{-1} of e^+e^- collisions, which includes the so-called *XYZ* data sample [23, 24] and the *R*-scan data sample [25], collected at CM energies from 3.80 to 4.95 GeV with the BESIII detector [26] at the BEPCII collider [27].

In order to achieve a high efficiency for the selection of $e^+e^- \rightarrow D\bar{D}$ events, we employ a single tag technique instead of a full reconstruction. With this technique we reconstruct only one $D^0(D^+)$ meson through the $K^-\pi^+\pi^+\pi^-(K^-\pi^+\pi^+)$ mode, while the corresponding anti-particle $\bar{D}^0(D^-)$ is extracted from the recoil side. Unless otherwise noted, the charge-conjugate mode of the $D^0(D^+)$ process is included by default. To determine the detection efficiency for $e^+e^- \rightarrow D\bar{D}$, 50,000 simulated events are generated for each energy point using the KKMC generator [28, 29] according to the VSS model [30, 31], where the ISR effect is included. The $D^0(D^+)$ meson decays to the $K^-\pi^+\pi^+\pi^-(K^-\pi^+\pi^+)$ modes are simulated with the amplitude sampling [32] via EVTGEN [30, 31], and the anti-mesons are set to decay inclusively according to the known branching fractions provided by PDG [2]. The response of the BESIII detector is modeled with Monte Carlo (MC) simulation using a framework based on GEANT4 [33, 34].

Charged tracks are reconstructed in the main drift chamber (MDC) with points of closest approach to the e^+e^- interaction point that are within 10 cm in the beam direction and 1 cm transverse to the beam direction and within the angular coverage of the MDC $|\cos\theta| < 0.93$, where θ is the polar angle with respect to the symmetry axis of the MDC. Information from the specific ionization energy loss measured in the MDC, combined with the time of flight, is used to determine the particle identification (PID) confidence levels for the pion and kaon hypotheses. Each track is assigned to the particle type with the higher probability. For the D^0 mode, events with at least one negatively charged kaon, one negatively charged pion, and two positively charged pions are kept for further analysis, for the D^+ mode, events with at least one negatively-charged kaon and two positively-charged pions for the D^+ mode, are kept for further analysis. The $D^0(D^+)$ candidates are reconstructed from the $K^-\pi^+\pi^+\pi^-(K^-\pi^+\pi^+)$ combination by requiring its invariant mass to be within 14 (16) MeV/ c^2 around the nominal $D^0(D^+)$ mass, which corresponds to three times the mass resolution.

The anti-meson candidates $\bar{D}^0(D^-)$ are inferred by the mass recoiling against the tagged meson (M_D^{recoil}) via the $K^-\pi^+\pi^+\pi^-(K^-\pi^+\pi^+)$ system:

$$M_D^{\text{recoil}} = \sqrt{(\sqrt{s} - E_D)^2 - |\mathbf{p}_D|^2}, \quad (1)$$

where E_D and \mathbf{p}_D are the energy and momentum of the selected $K^-\pi^+\pi^+\pi^-(K^-\pi^+\pi^+)$ candidate in the CM system, and \sqrt{s} is the CM energy [35]. To improve the resolution, a correction is applied to M_D^{recoil} given by $M_D^{\text{recoil}} + M_D - m_D$, where M_D is the invariant mass of the selected $K^-\pi^+\pi^+\pi^-(K^-\pi^+\pi^+)$ candidate and m_D is the nominal D mass [2]. Figure 1 shows the 2D distributions of M_D^{recoil} versus M_D for the $K^-\pi^+\pi^+\pi^-(K^-\pi^+\pi^+)$ final states at $\sqrt{s} = 4.1992$ GeV. After applying all the aforementioned selection criteria, the remaining background exhibits a smooth shape in the region of interest based on the sideband study.

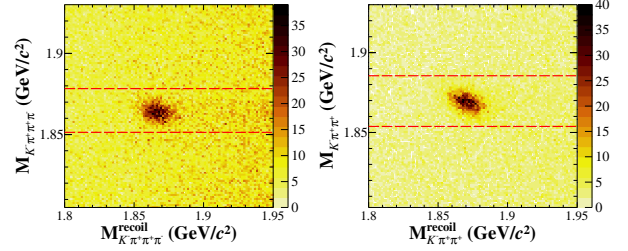


FIG. 1. The two-dimensional distributions of M_D versus M_D^{recoil} at $\sqrt{s} = 4.1992$ GeV. The dashed lines represent the signal region for the D meson in the $D^0\bar{D}^0$ mode (left) and the D^+D^- mode (right).

The signal yields for the $e^+e^- \rightarrow D\bar{D}$ process at each energy point are extracted by performing an extended maximum likelihood fit to the M_D^{recoil} spectrum in the range from 1.80 GeV/ c^2 to 1.95 GeV/ c^2 . In the fit, the signal shape for the $e^+e^- \rightarrow D\bar{D}$ process is described by the convolution of the MC-simulated shape with a Gaussian function, which accounts for the difference in mass resolution between the data and the MC-simulation. The parameters of the Gaussian function are floating for *XYZ* data points and some *R*-scan data points with higher statistics, while they are fixed for the other *R*-scan data points with low statistics. The fixed parameters are determined from the fits to the neighbor *XYZ* data points. The background contributions are modeled using a second-order polynomial function. Figure 2 illustrates the results of the fits to the M_D^{recoil} distributions at $\sqrt{s} = 4.1992$ GeV. The signal yields obtained from the fits are summarized in the supplemental material at [36].

The Born cross section for $e^+e^- \rightarrow D\bar{D}$ is calculated by

$$\sigma^B(s) = \frac{N_{\text{obs}}}{2\mathcal{L}(1+\delta)\frac{1}{|1-\Pi|^2}\epsilon\mathcal{B}}, \quad (2)$$

where N_{obs} represents the number of observed signal events, the factor of 2 accounts for the charge-conjugate mode, \mathcal{L} corresponds to the integrated luminosity, $(1+\delta)$ is the ISR correction factor, $\frac{1}{|1-\Pi|^2}$ is the vacuum polarization correction

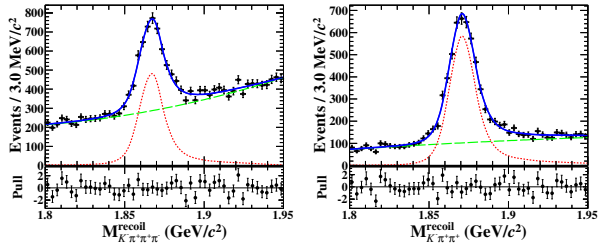


FIG. 2. Fits to the M_D^{recoil} spectra at $\sqrt{s} = 4.1992$ GeV for the $D^0\bar{D}^0$ mode (left) and the D^+D^- mode (right). The dots with error bars represent the data, the blue solid lines indicate the fit results, the red short-dashed lines represent the signal, and the green long-dashed lines correspond to the background.

factor [37], ϵ denotes the detection efficiency, and \mathcal{B} stands for the branching fractions of $D^0 \rightarrow K^-\pi^+\pi^+\pi^-$ mode and $D^+ \rightarrow K^-\pi^+\pi^+$ mode, taken from the Particle Data Group [2]. The ISR correction factor is obtained through QED calculations [38], where the cross sections measured in this analysis are used as inputs and iterated until convergence. The measured Born cross sections, along with the results from the CLEO-c [22], BaBar [20], and Belle [21] experiments, are shown in Fig. 3 and summarized in Ref. [36], which also includes all the numbers used in the calculation.

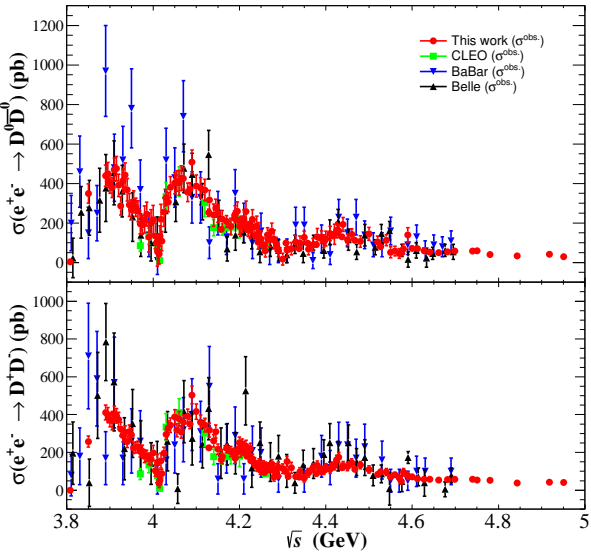


FIG. 3. Cross sections with total uncertainties for the $e^+e^- \rightarrow D\bar{D}$ process as a function of CM energy from 3.80 to 4.95 GeV compared between this work (Born) and the previous measurements (observed).

A least- χ^2 method is used to perform a simultaneous fit of the dressed cross sections $\sigma^{\text{dressed}} = \sigma^B / [1 - \prod_i |^2]$ for the $e^+e^- \rightarrow D^0\bar{D}^0$ and D^+D^- processes, parameterized as the coherent sum of eight relativistic Breit-Wigner (BW) func-

tions:

$$\sigma^{\text{dressed}}(\sqrt{s}) = \left| \sum_{i=1}^9 e^{i\phi} BW_i(\sqrt{s}) \sqrt{\frac{P(\sqrt{s})}{P(M)}} \right|^2, \quad (3)$$

where $BW(\sqrt{s})$ is given by

$$BW(\sqrt{s}) = \frac{\sqrt{12\pi\Gamma_{ee}\mathcal{B}\Gamma}}{s - M^2 + iM\Gamma}. \quad (4)$$

Here, the masses, M , and total widths, Γ , for seven known resonances $\psi(3770)$, $\psi(4040)$, $\psi(4160)$, $Y(4230)$, $Y(4360)$, $\psi(4415)$, and $Y(4660)$ are fixed at individual PDG values [2], while they are free for another resonance regarded as R around $3.9 \text{ GeV}/c^2$. For Γ_{ee} , electronic partial widths, and \mathcal{B} , the branching fractions of the decay, they are free for all resonances. Note that the effect for fixing resonance parameters is studied by varying the fixed values by 1σ uncertainty, and can be ignored. The relative phase between different BW functions is denoted by ϕ , which is set to be different in the simultaneous fit for both modes. And $P(\sqrt{s})$ represents the two-body phase space factor. To account for the beam energy spread, $\sigma^{\text{dressed}}(\sqrt{s})$ is convolved with a Gaussian function with the standard deviation $\sigma = -2.147 + 0.9454 \cdot \sqrt{s}$. The significances for R , calculated by comparing the χ^2 values and the degrees of freedom (d.o.f) with and without their inclusion in the fit, are greater than 20σ , taking into account the systematic uncertainty. The other assumed resonances are all observed, except for evidence for $\psi(4415)$ with a significance of 4.0σ including the systematic uncertainty. Figure 4 shows the result of one solution of the simultaneous fit to the dressed cross sections for the $e^+e^- \rightarrow D\bar{D}$ process with the assumption of eight resonances in the energy range from 3.80 to 4.95 GeV. Table I summarizes the numerical results from the fit. Note that according to the methods described in Refs. [39, 40], there should be at least one hundred and twenty-eight multiple solutions. For simplicity, only the range of the central values for $\Gamma_{ee}\mathcal{B}$ is provided. And also the resonance parameters for R strongly depend on the chosen fit model, indicating the need for further in-depth research.

Systematic uncertainties in the measurement of the cross sections for the $e^+e^- \rightarrow D^0\bar{D}^0$ and D^+D^- processes originate from the luminosity measurement, the efficiencies of tracking and PID, the requirement of the D mass window, the fit of the M_D^{recoil} spectrum, the branching fractions of $D^0 \rightarrow K^-\pi^+\pi^+\pi^-$ and $D^+ \rightarrow K^-\pi^+\pi^+$, and the line-shape structures. The uncertainty due to the vacuum polarization is negligible. The integral luminosity is measured to an uncertainty up to 1.0% [23]. The uncertainties due to data-MC differences in BESIII tracking and particle ID efficiencies are both 1% per track [41]. The requirement of the D mass window is studied by varying the nominal requirements by $\pm 1\sigma$, resulting in uncertainties of 2.1% and 1.8% in the neutral and charged modes, respectively. The systematic uncertainty arising from the fit of the M_D^{recoil} spectrum includes the fit range and the background shape. Varying the mass range by

TABLE I. Fit results of the Born cross section, where the first uncertainties are the statistical and the second are systematic and S denotes the significance.

$e^+e^- \rightarrow D\bar{D}$								
Resonance	$\psi(3770)$	R	$\psi(4040)$	$\psi(4160)$	$Y(4230)$	$Y(4360)$	$\psi(4415)$	$Y(4660)$
Mass (MeV/c ²)	3773.7 (fixed)	$3872.5 \pm 14.2 \pm 3.0$	4039 (fixed)	4191 (fixed)	4222.5 (fixed)	4374 (fixed)	4421 (fixed)	4630 (fixed)
Width (MeV/c ²)	87.6 (fixed)	$179.7 \pm 14.1 \pm 7.0$	80 (fixed)	70 (fixed)	48 (fixed)	118 (fixed)	62 (fixed)	72 (fixed)
$\Gamma_{ee}B$ (eV)	95-106	202-292	41-44	1-2	1-2	50-144	0-2	0-1
S(σ)	10	> 20	13	7	11	11	4	8
$\chi^2/\text{d.o.f}$	$= 346/275$							
p-value = 0.002								

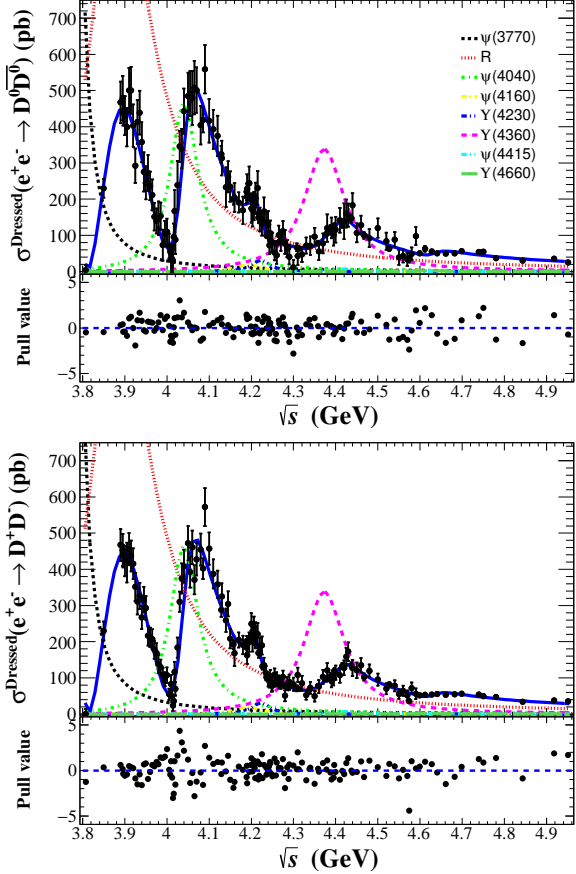


FIG. 4. One solution of the simultaneous fits to the dressed cross sections for the $e^+e^- \rightarrow D^0\bar{D}^0$ and $D^+\bar{D}^-$ processes with the assumption of eight resonances.

± 5 MeV/c² results in an uncertainty of 1.5% for the neutral mode and 1.6% for the charged mode. The uncertainty due to the background shape is estimated to be 1.0% for the neutral mode and 0.9% for the charged mode using alternative fits with a second or third-order polynomial function. The branching fractions of $D^0 \rightarrow K^-\pi^+\pi^+\pi^-$ and $D^+ \rightarrow K^-\pi^+\pi^+$ are quoted with uncertainties of 2.4% for both modes from the PDG [2]. The uncertainty arising from the line-shape model, including the ISR correction factor, is estimated by comparing the $(1 + \delta) \cdot \epsilon$ values with and without the addition of one more resonance in the fit of the cross sections as the input line shape, which introduces an uncertainty of 1.5% for the neutral mode

and 1.6% for the charged mode between the nominal and alternative models. Assuming all sources are independent, the total systematic uncertainties on the cross sections measurements are determined to be 7.0% for the $e^+e^- \rightarrow D^0\bar{D}^0$ mode and 6.5% for the $e^+e^- \rightarrow D^+\bar{D}^-$ mode by quadratic sum.

Systematic uncertainties on the measurement of the resonance parameters mainly arise from the uncertainties in the CM energy calibration and the presence of multiple solutions. A systematic uncertainty of 0.8 MeV [35] is assigned to account for the uncertainties in the CM energy, and this uncertainty is propagated to the mass and width of R . The systematic uncertainties associated with multiple solutions are determined by comparing the resonance parameters between the nominal solution and the one that exhibits the largest difference. Other uncertainties arising from the measurement of Born cross sections have been accounted for by incorporating them into the line-shape fit.

In summary, a measurement of exclusive Born cross sections for the $e^+e^- \rightarrow D^0\bar{D}^0$ and $D^+\bar{D}^-$ processes is presented at 150 CM energy points ranging from 3.80 to 4.95 GeV with unprecedented precision. The result is in qualitative agreement with previous experiments [20–22] and the prediction of the coupled-channel model [1]. A simultaneous fit to the dressed cross sections for $e^+e^- \rightarrow D^0\bar{D}^0$ and $D^+\bar{D}^-$ is performed assuming eight resonances, including R , $\psi(3770)$, $\psi(4040)$, $\psi(4160)$, $Y(4230)$, $Y(4360)$, $\psi(4415)$, and $Y(4660)$. One potential new structure, denoted as R , is observed around the mass values of 3.9 GeV/c². All other known resonances are also observed in the $D\bar{D}$ final states, except for an evidence for $\psi(4415)$ with a significance of 4.0σ . Our results are important to identify possible explanations for the nature of charmonium-like states produced above the open-charm threshold, such as $Y(4230)$, $Y(4360)$, and $Y(4660)$. In the theoretical prediction if these states are pure 1⁻⁺ charmonium states, they should predominantly decay into the $D\bar{D}$ final state [42–46]. Our results may favor the notion that these resonances $Y(4230)$, $Y(4360)$, and $Y(4660)$ are the scenario of pure conventional charmonium states. However, due to experimental limitations, our results for describing the line shape provided in this work depend on the chosen model, indicating the need for further in-depth research. This work provides important experimental evidences with unprecedented precision and insights into the nature above the open-charm region, especially for the under-

standing of the property of charmonium-like states.

ACKNOWLEDGEMENT

The BESIII Collaboration thanks the staff of BEPCII and the IHEP computing center for their strong support. This work is supported in part by National Key R&D Program of China under Contracts Nos. 2020YFA0406300, 2020YFA0406400; National Natural Science Foundation of China (NSFC) under Contracts Nos. 12075107, 12247101, 11635010, 11735014, 11835012, 11935015, 11935016, 11935018, 11961141012, 12022510, 12025502, 12035009, 12035013, 12061131003, 12192260, 12192261, 12192262, 12192263, 12192264, 12192265, 12221005, 12225509, 12235017; the 111 Project under Grant No. B20063; the Chinese Academy of Sciences (CAS) Large-Scale Scientific Facility Program; the CAS Center for Excellence in Particle Physics (CCEPP); Joint Large-Scale Scientific Facility Funds of the NSFC and CAS under Contract No. U1832207; CAS Key Research Program of Frontier Sciences under Contracts Nos. QYZDJ-SSW-SLH003, QYZDJ-SSW-SLH040; 100 Talents Program of CAS; The Institute of Nuclear and Particle Physics (IN-PAC) and Shanghai Key Laboratory for Particle Physics and Cosmology; European Union's Horizon 2020 research and innovation programme under Marie Skłodowska-Curie grant agreement under Contract No. 894790; German Research Foundation DFG under Contracts Nos. 455635585, Collaborative Research Center CRC 1044, FOR5327, GRK 2149; Istituto Nazionale di Fisica Nucleare, Italy; Ministry of Development of Turkey under Contract No. DPT2006K-120470; National Research Foundation of Korea under Contract No. NRF-2022R1A2C1092335; National Science and Technology fund of Mongolia; National Science Research and Innovation Fund (NSRF) via the Program Management Unit for Human Resources & Institutional Development, Research and Innovation of Thailand under Contract No. B16F640076; Polish National Science Centre under Contract No. 2019/35/O/ST2/02907; The Swedish Research Council; U. S. Department of Energy under Contract No. DE-FG02-05ER41374.

- [7] G. Pakhlova *et al.* (Belle Collaboration), *Phys. Rev. Lett.* **101**, 172001 (2008).
- [8] J. P. Lees *et al.* (BaBar Collaboration), *Phys. Rev. D* **86**, 051102(R) (2012).
- [9] Z. Q. Liu *et al.* (Belle Collaboration), *Phys. Rev. Lett.* **110**, 252002 (2013).
- [10] J. P. Lees *et al.* (BaBar Collaboration), *Phys. Rev. D* **89**, 111103(R) (2014).
- [11] X. L. Wang *et al.* (Belle Collaboration), *Phys. Rev. D* **91**, 112007 (2015).
- [12] T. E. Coan *et al.* (CLEO Collaboration), *Phys. Rev. Lett.* **96**, 162003 (2006).
- [13] M. Ablikim *et al.* (BESIII Collaboration), *Phys. Rev. Lett.* **114**, 092003 (2015).
- [14] M. Ablikim *et al.* (BESIII Collaboration), *Phys. Rev. Lett.* **118**, 092001 (2017).
- [15] M. Ablikim *et al.* (BESIII Collaboration), *Phys. Rev. Lett.* **118**, 092002 (2017).
- [16] M. Ablikim *et al.* (BESIII Collaboration), *Phys. Rev. Lett.* **124**, 032002 (2020).
- [17] M. Ablikim *et al.* (BESIII Collaboration), *Phys. Rev. D* **104**, L091104 (2021).
- [18] H. X. Chen, W. Chen, X. Liu and S. L. Zhu, *Phys. Rep.* **639**, 1 (2016).
- [19] N. Brambilla, S. Eidelman, C. Hanhart, A. Nefediev, C. P. Shen, C. E. Thomas, A. Vairo and C. Z. Yuan, *Phys. Rept.* **873**, 1-154 (2020).
- [20] B. Aubert *et al.* (BaBar Collaboration), *Phys. Rev. D* **76**, 111105(R) (2007).
- [21] G. Pakhlova *et al.* (Belle Collaboration), *Phys. Rev. D* **77**, 011103(R) (2008).
- [22] D. Cronin-Hennessy *et al.* (CLEO Collaboration), *Phys. Rev. D* **80**, 072001 (2009).
- [23] M. Ablikim *et al.* (BESIII Collaboration), *Chin. Phys. C* **39**, 093001 (2015).
- [24] M. Ablikim *et al.* (BESIII Collaboration), *Chin. Phys. C* **46**, 113002 (2022).
- [25] M. Ablikim *et al.* (BESIII Collaboration), *Chin. Phys. C* **41**, 063001 (2017).
- [26] Y. F. Wang, *Int. J. Mod. Phys. A* **21**, 5371 (2006).
- [27] M. Ablikim *et al.* (BESIII Collaboration), *Nucl. Instrum. Meth. A* **614**, 345 (2010).
- [28] S. Jadach, B. F. L. Ward and Z. Was, *Comput. Phys. Commun.* **130**, 260 (2000).
- [29] S. Jadach, B. F. L. Ward and Z. Was, *Phys. Rev. D* **63**, 113009 (2001).
- [30] D. J. Lange, *Nucl. Instrum. Meth. A* **462**, 152 (2001).
- [31] R. G. Ping, *Chin. Phys. C* **32**, 599 (2008).
- [32] M. Ablikim *et al.* (BESIII Collaboration), *Phys. Rev. D* **95**, 072010 (2017).
- [33] S. Agostinelli *et al.* (GEANT4 Collaboration), *Nucl. Instrum. Meth. A* **506**, 250 (2003).
- [34] J. Allison *et al.*, *IEEE Trans. Nucl. Sci.* **53**, 270 (2006).
- [35] M. Ablikim *et al.* (BESIII Collaboration), *Chin. Phys. C* **45**, 103001 (2021).
- [36] See Supplemental Material at <http://XXXadd later for a summary of number of signal events, luminosity, detection efficiency, ISR correction factor, vacuum polarization factor and Born cross section at each energy point and Multi-solutions>.
- [37] S. Actis *et al.*, *Eur. Phys. J. C* **66**, 585 (2010).
- [38] S. Jadach, B. F. L. Ward and Z. Was, *Phys. Rev. D* **63**, 113009 (2001).
- [39] K. Zhu, X. H. Mo, C. Z. Yuan, and P. Wang, *Int. J. Mod. Phys. A* **26**, 4511 (2011).

- [40] Y. Bai and D. Y. Chen, *Phys. Rev. D* **99**, 072007 (2019).
- [41] M. Ablikim *et al.* (BESIII Collaboration), *Phys. Rev. D* **101**, 112008 (2020).
- [42] J. Z. Wang, D. Y. Chen, X. Liu and T. Matsuki, *Phys. Rev. D* **99**, 114003 (2019).
- [43] J. Z. Wang, R. Q. Qian, X. Liu and T. Matsuki, *Phys. Rev. D* **101**, 034001 (2020).
- [44] F. J. Llanes-Estrada, *Phys. Rev. D* **72**, 031503(R) (2005)
- [45] B. Q. Li, K. T. Chao, *Phys. Rev. D* **79**, 094004 (2009).
- [46] Q. F. Cao, H. R. Qi, G. Y. Tang, *et al.*, *Eur. Phys. J. C* **81**, 83 (2010).

Supplemental Material

\sqrt{s} (GeV)	\mathcal{L} (pb^{-1})	$(1 + \delta)$	$\frac{1}{ 1 - \Pi ^2}$	ϵ	N_{obs}	σ^B (pb)
3.80765	50.540	0.87	1.06	0.52	13.8 ± 48.4	$3.8 \pm 13.4 \pm 0.3$
3.85000	7.967	1.15	1.05	0.41	179.5 ± 21.9	$288.8 \pm 35.2 \pm 20.2$
3.89000	7.758	0.94	1.05	0.41	219.3 ± 22.2	$445.3 \pm 45.1 \pm 31.2$
3.89500	7.567	0.94	1.05	0.41	221.6 ± 23.7	$456.1 \pm 48.8 \pm 31.9$
3.89624	52.610	0.94	1.05	0.43	1458.5 ± 59.3	$417.8 \pm 17.0 \pm 29.2$
3.90000	7.575	0.93	1.05	0.41	199.4 ± 20.6	$410.2 \pm 42.4 \pm 28.7$
3.90500	7.596	0.95	1.05	0.42	189.9 ± 21.5	$380.0 \pm 43.1 \pm 26.6$
3.91000	7.240	0.94	1.05	0.41	222.6 ± 23.0	$476.6 \pm 49.3 \pm 33.4$
3.91500	7.454	0.95	1.05	0.42	237.6 ± 26.0	$476.7 \pm 52.1 \pm 33.4$
3.92000	6.806	0.97	1.05	0.42	175.9 ± 22.4	$383.7 \pm 48.9 \pm 26.9$
3.92500	6.694	0.98	1.05	0.42	125.6 ± 18.4	$278.6 \pm 40.7 \pm 19.5$
3.93000	6.735	1.00	1.05	0.41	180.4 ± 23.2	$393.5 \pm 50.5 \pm 27.5$
3.93500	7.161	1.01	1.05	0.41	203.7 ± 24.1	$418.1 \pm 49.4 \pm 29.3$
3.94000	7.228	1.03	1.05	0.40	168.8 ± 23.4	$340.4 \pm 47.2 \pm 23.8$
3.94500	7.590	1.06	1.05	0.40	139.4 ± 25.6	$262.0 \pm 48.2 \pm 18.3$
3.95000	7.714	1.09	1.05	0.39	128.5 ± 22.3	$233.4 \pm 40.5 \pm 16.3$
3.95500	8.124	1.13	1.05	0.38	150.9 ± 25.2	$259.3 \pm 43.4 \pm 18.2$
3.96000	8.489	1.18	1.05	0.38	141.2 ± 21.2	$225.5 \pm 33.8 \pm 15.8$
3.96500	7.768	1.23	1.05	0.37	118.9 ± 22.6	$201.5 \pm 38.3 \pm 14.1$
3.97000	7.321	1.29	1.05	0.36	80.0 ± 19.4	$144.1 \pm 35.0 \pm 10.1$
3.97500	8.062	1.37	1.05	0.34	83.7 ± 20.0	$133.1 \pm 31.8 \pm 9.3$
3.98000	6.486	1.48	1.05	0.34	75.2 ± 23.0	$140.2 \pm 42.9 \pm 9.8$
3.98500	7.969	1.60	1.05	0.31	95.7 ± 22.7	$145.8 \pm 34.5 \pm 10.2$
3.99000	8.024	1.76	1.05	0.30	48.4 ± 28.1	$69.5 \pm 40.3 \pm 4.9$
3.99500	7.985	1.91	1.05	0.28	71.4 ± 23.2	$100.2 \pm 32.5 \pm 7.0$
4.00000	7.732	1.98	1.05	0.27	70.7 ± 23.0	$104.5 \pm 34.1 \pm 7.3$
4.00500	7.537	1.92	1.04	0.26	42.2 ± 20.2	$67.5 \pm 32.3 \pm 4.7$
4.00762	482.000	1.83	1.04	0.26	1999.4 ± 207.3	$52.6 \pm 5.5 \pm 3.7$
4.01000	7.183	1.71	1.04	0.27	17.1 ± 22.8	$31.4 \pm 41.8 \pm 2.2$
4.01200	6.907	1.61	1.04	0.27	16.8 ± 18.8	$33.4 \pm 37.4 \pm 2.3$
4.01400	6.694	1.50	1.04	0.29	13.0 ± 15.0	$27.7 \pm 31.9 \pm 1.9$
4.01600	6.544	1.40	1.04	0.29	40.8 ± 15.6	$91.8 \pm 35.2 \pm 6.4$
4.01800	6.968	1.31	1.04	0.30	72.9 ± 24.9	$160.2 \pm 54.6 \pm 11.2$
4.02000	6.726	1.23	1.04	0.31	36.0 ± 16.0	$84.6 \pm 37.5 \pm 5.9$
4.02500	6.538	1.07	1.05	0.34	89.4 ± 24.4	$227.4 \pm 62.0 \pm 15.9$
4.03000	16.451	0.95	1.05	0.37	313.2 ± 32.4	$329.3 \pm 34.1 \pm 23.1$
4.03500	6.706	0.90	1.05	0.39	126.4 ± 18.3	$323.2 \pm 46.8 \pm 22.6$
4.04000	6.564	0.86	1.05	0.41	159.8 ± 19.5	$421.8 \pm 51.6 \pm 29.5$
4.05000	6.567	0.83	1.05	0.42	175.8 ± 19.9	$461.4 \pm 52.3 \pm 32.3$
4.05500	6.927	0.84	1.05	0.42	190.9 ± 20.2	$467.7 \pm 49.6 \pm 32.7$
4.06000	6.338	0.84	1.05	0.43	172.9 ± 24.0	$457.2 \pm 63.6 \pm 32.0$
4.06500	7.022	0.84	1.05	0.43	203.7 ± 25.9	$483.9 \pm 61.5 \pm 33.9$
4.07000	7.271	0.85	1.05	0.43	211.8 ± 22.0	$477.3 \pm 49.5 \pm 33.4$
4.08000	7.721	0.88	1.05	0.43	184.6 ± 20.7	$385.1 \pm 43.2 \pm 27.0$
4.08545	52.860	0.89	1.05	0.43	1340.8 ± 56.7	$399.0 \pm 16.9 \pm 27.9$
4.09000	7.611	0.91	1.05	0.43	261.0 ± 25.3	$532.6 \pm 51.7 \pm 37.3$
4.10000	7.254	0.93	1.05	0.42	188.1 ± 23.8	$396.7 \pm 50.2 \pm 27.8$
4.11000	7.146	0.96	1.05	0.42	177.2 ± 20.9	$374.3 \pm 44.2 \pm 26.2$
4.12000	7.648	0.98	1.05	0.42	183.2 ± 24.1	$356.6 \pm 46.8 \pm 25.0$
4.12878	401.500	0.78	1.05	0.47	7468.6 ± 145.7	$308.5 \pm 6.0 \pm 21.6$
4.13000	7.207	1.01	1.05	0.40	145.6 ± 19.8	$298.5 \pm 40.6 \pm 20.9$
4.14000	7.268	1.03	1.05	0.39	108.2 ± 24.3	$222.0 \pm 49.9 \pm 15.5$
4.14500	7.774	1.05	1.05	0.39	130.4 ± 19.5	$249.6 \pm 37.2 \pm 17.5$

4.15000	7.662	1.06	1.05	0.39	116.0 ± 19.1	223.5 ± 36.8 ± 15.6
4.15783	408.700	0.84	1.05	0.46	5040.5 ± 150.1	190.6 ± 5.7 ± 13.3
4.16000	7.954	1.08	1.05	0.38	104.8 ± 19.1	194.4 ± 35.4 ± 13.6
4.17000	18.008	1.09	1.05	0.37	217.1 ± 27.5	181.8 ± 23.0 ± 12.7
4.18000	7.309	1.08	1.05	0.37	77.3 ± 16.6	161.1 ± 34.5 ± 11.3
4.18859	43.330	1.08	1.06	0.37	598.5 ± 47.0	207.6 ± 16.3 ± 14.5
4.18912	526.700	1.08	1.06	0.36	6645.6 ± 158.1	195.0 ± 4.6 ± 13.6
4.19000	7.560	1.07	1.06	0.37	107.5 ± 17.6	215.4 ± 35.2 ± 15.1
4.19500	7.503	1.06	1.06	0.37	112.2 ± 19.3	230.5 ± 39.7 ± 16.1
4.19915	526.000	1.06	1.06	0.36	6434.5 ± 155.1	189.5 ± 4.6 ± 13.3
4.20000	7.582	1.06	1.06	0.37	81.8 ± 17.6	164.7 ± 35.5 ± 11.5
4.20300	4.734	1.07	1.06	0.37	49.7 ± 12.8	160.1 ± 41.1 ± 11.2
4.20600	7.638	1.07	1.06	0.36	83.5 ± 17.0	170.2 ± 34.7 ± 11.9
4.20773	54.950	1.07	1.06	0.37	648.4 ± 50.3	177.3 ± 13.8 ± 12.4
4.20939	517.100	1.09	1.06	0.35	6218.4 ± 148.9	186.9 ± 4.5 ± 13.1
4.21000	7.678	1.09	1.06	0.36	96.1 ± 19.4	191.1 ± 38.6 ± 13.4
4.21500	7.768	1.12	1.06	0.36	112.9 ± 21.6	217.6 ± 41.6 ± 15.2
4.21713	54.600	1.15	1.06	0.36	529.8 ± 44.2	140.8 ± 11.7 ± 9.9
4.21893	514.600	1.16	1.06	0.34	5234.2 ± 142.5	153.3 ± 4.2 ± 10.7
4.22000	7.935	1.18	1.06	0.34	72.7 ± 15.7	135.5 ± 29.3 ± 9.5
4.22500	8.212	1.24	1.06	0.33	70.6 ± 16.4	123.9 ± 28.8 ± 8.7
4.22626	1100.940	1.26	1.06	0.34	10355.1 ± 206.7	133.1 ± 2.7 ± 9.3
4.23000	8.193	1.31	1.06	0.33	91.7 ± 20.0	157.0 ± 34.2 ± 11.0
4.23500	8.273	1.36	1.06	0.32	74.8 ± 15.3	125.4 ± 25.7 ± 8.8
4.23577	530.300	1.37	1.06	0.31	3621.0 ± 131.5	94.5 ± 3.4 ± 6.6
4.24000	7.830	1.41	1.06	0.31	69.4 ± 19.1	122.6 ± 33.7 ± 8.6
4.24166	55.880	1.43	1.06	0.31	374.8 ± 45.4	90.9 ± 11.0 ± 6.4
4.24300	8.571	1.42	1.06	0.30	40.8 ± 13.7	68.7 ± 23.1 ± 4.8
4.24397	538.100	1.43	1.06	0.30	3301.7 ± 117.3	84.2 ± 3.0 ± 5.9
4.24500	8.487	1.44	1.06	0.30	60.6 ± 19.7	99.7 ± 32.4 ± 7.0
4.24800	8.554	1.45	1.06	0.30	46.0 ± 15.1	75.0 ± 24.6 ± 5.2
4.25000	8.596	1.48	1.05	0.30	48.0 ± 15.3	77.0 ± 24.5 ± 5.4
4.25500	8.657	1.69	1.05	0.28	33.7 ± 13.7	49.9 ± 20.3 ± 3.5
4.25797	828.400	1.15	1.05	0.37	4280.2 ± 145.9	73.3 ± 2.9 ± 5.1
4.26000	8.880	1.32	1.05	0.30	25.0 ± 13.3	43.0 ± 22.9 ± 3.0
4.26500	8.629	1.39	1.05	0.29	55.7 ± 14.0	95.6 ± 24.0 ± 6.7
4.26681	531.100	1.40	1.05	0.29	2834.6 ± 122.9	78.2 ± 3.4 ± 5.5
4.27000	7.522	1.41	1.05	0.28	41.2 ± 13.9	82.1 ± 27.7 ± 5.7
4.27500	8.567	1.43	1.05	0.28	60.3 ± 15.1	105.5 ± 26.4 ± 7.4
4.27778	175.700	1.45	1.05	0.28	890.5 ± 65.3	75.6 ± 5.5 ± 5.3
4.28000	8.723	1.44	1.05	0.28	45.6 ± 17.9	77.6 ± 30.5 ± 5.4
4.28500	8.596	1.46	1.05	0.27	34.4 ± 12.6	60.7 ± 22.2 ± 4.2
4.28843	502.400	1.04	1.05	0.37	2082.8 ± 112.0	64.9 ± 3.5 ± 4.5
4.29000	9.010	1.48	1.05	0.28	23.5 ± 11.9	38.5 ± 19.4 ± 2.7
4.30000	8.453	1.49	1.05	0.27	6.2 ± 10.8	11.2 ± 19.3 ± 0.8
4.30789	45.080	1.48	1.05	0.27	191.4 ± 28.6	63.6 ± 9.5 ± 4.5
4.31000	8.599	1.49	1.05	0.27	23.0 ± 13.4	40.5 ± 23.6 ± 2.8
4.31268	501.200	1.05	1.05	0.36	1928.5 ± 109.0	60.6 ± 3.4 ± 4.2
4.32000	9.342	1.49	1.05	0.26	26.9 ± 11.8	44.8 ± 19.7 ± 3.1
4.33000	8.657	1.46	1.05	0.26	37.6 ± 11.4	68.4 ± 20.8 ± 4.8
4.33793	505.000	1.01	1.05	0.37	2091.6 ± 103.8	66.6 ± 3.3 ± 4.7
4.34000	8.700	1.39	1.05	0.27	37.2 ± 13.0	67.8 ± 23.8 ± 4.7
4.35000	8.542	1.32	1.05	0.28	48.7 ± 11.8	91.7 ± 22.3 ± 6.4
4.35826	543.900	1.24	1.05	0.30	2528.0 ± 115.3	74.8 ± 3.4 ± 5.2
4.36000	8.063	1.23	1.05	0.30	25.7 ± 10.8	52.7 ± 22.1 ± 3.7
4.37000	8.498	1.16	1.05	0.31	37.7 ± 13.2	73.8 ± 25.8 ± 5.2
4.37788	522.700	0.88	1.05	0.40	3034.5 ± 111.3	98.7 ± 3.6 ± 6.9
4.38000	8.158	1.09	1.05	0.32	54.7 ± 16.8	114.3 ± 35.1 ± 8.0
4.38740	55.570	1.07	1.05	0.35	376.8 ± 34.4	109.8 ± 10.0 ± 7.7
4.39000	7.460	1.07	1.05	0.34	51.3 ± 11.8	114.6 ± 26.3 ± 8.0
4.39500	7.430	1.06	1.05	0.35	43.7 ± 12.6	96.5 ± 27.7 ± 6.8
4.39683	507.800	0.87	1.05	0.41	3560.4 ± 100.6	118.3 ± 3.3 ± 8.3
4.40000	7.178	1.05	1.05	0.35	48.0 ± 14.4	110.0 ± 33.0 ± 7.7
4.41000	6.352	1.04	1.05	0.35	52.1 ± 12.1	134.8 ± 31.4 ± 9.4

4.41558	1090.700	1.03	1.05	0.37	8449.0 \pm 151.8	124.0 \pm 2.2 \pm 8.7
4.42000	7.519	1.03	1.05	0.36	61.8 \pm 21.4	132.5 \pm 46.0 \pm 9.3
4.42500	7.436	1.02	1.05	0.36	69.8 \pm 16.1	152.7 \pm 35.2 \pm 10.7
4.43000	6.788	1.03	1.05	0.37	63.0 \pm 12.1	148.5 \pm 28.6 \pm 10.4
4.43710	569.900	0.89	1.05	0.42	4923.1 \pm 151.6	140.0 \pm 4.3 \pm 9.8
4.44000	7.638	1.05	1.05	0.36	83.6 \pm 14.1	174.5 \pm 29.5 \pm 12.2
4.45000	7.677	1.08	1.05	0.36	50.3 \pm 12.1	101.9 \pm 24.4 \pm 7.1
4.46000	8.724	1.11	1.05	0.35	68.7 \pm 13.1	122.2 \pm 23.2 \pm 8.6
4.46706	111.090	1.13	1.05	0.35	688.9 \pm 44.9	94.9 \pm 6.2 \pm 6.6
4.48000	8.167	1.16	1.05	0.34	46.6 \pm 12.3	87.6 \pm 23.0 \pm 6.1
4.50000	7.997	1.21	1.05	0.33	59.7 \pm 12.6	114.6 \pm 24.2 \pm 8.0
4.52000	8.674	1.25	1.05	0.31	44.6 \pm 12.1	79.6 \pm 21.6 \pm 5.6
4.52714	112.120	1.26	1.05	0.31	439.5 \pm 39.2	60.3 \pm 5.4 \pm 4.2
4.54000	9.335	1.29	1.05	0.30	50.6 \pm 11.8	83.6 \pm 19.5 \pm 5.8
4.55000	8.765	1.32	1.05	0.30	21.1 \pm 11.2	37.3 \pm 19.8 \pm 2.6
4.56000	8.259	1.35	1.05	0.29	21.7 \pm 9.0	40.8 \pm 16.9 \pm 2.9
4.57000	8.390	1.37	1.05	0.28	17.3 \pm 9.2	31.9 \pm 16.9 \pm 2.2
4.57450	48.930	1.39	1.05	0.29	106.4 \pm 27.0	32.4 \pm 8.2 \pm 2.3
4.58000	8.545	1.41	1.05	0.28	25.9 \pm 9.4	46.2 \pm 16.8 \pm 3.2
4.59000	8.162	1.43	1.05	0.27	48.8 \pm 11.9	93.4 \pm 22.8 \pm 6.5
4.59953	586.900	1.45	1.05	0.28	1851.7 \pm 103.3	47.5 \pm 2.6 \pm 3.3
4.61186	103.650	1.13	1.05	0.33	388.2 \pm 40.9	59.8 \pm 6.3 \pm 4.2
4.62800	521.520	1.08	1.05	0.34	1668.1 \pm 86.2	52.5 \pm 2.7 \pm 3.7
4.64091	552.410	1.04	1.05	0.35	1582.5 \pm 82.9	48.0 \pm 2.5 \pm 3.4
4.66124	529.630	1.02	1.05	0.35	1499.9 \pm 79.9	47.0 \pm 2.5 \pm 3.3
4.68192	1669.310	1.07	1.05	0.35	4972.8 \pm 126.8	47.7 \pm 1.2 \pm 3.3
4.69882	536.450	1.05	1.05	0.35	1739.8 \pm 79.5	53.1 \pm 2.4 \pm 3.7
4.73970	164.270	1.08	1.05	0.35	532.3 \pm 46.8	51.1 \pm 4.5 \pm 3.6
4.75005	367.210	1.09	1.05	0.35	1196.4 \pm 58.7	51.9 \pm 2.5 \pm 3.6
4.78054	512.780	1.11	1.06	0.34	1112.3 \pm 67.1	34.4 \pm 2.1 \pm 2.4
4.84307	527.290	1.14	1.06	0.33	936.7 \pm 71.6	28.1 \pm 2.1 \pm 2.0
4.91802	208.110	1.17	1.06	0.33	441.9 \pm 44.5	33.6 \pm 3.4 \pm 2.3
4.95093	160.370	1.18	1.06	0.31	228.8 \pm 34.5	23.2 \pm 3.5 \pm 1.6

TABLE II: The $e^+e^- \rightarrow D^0\bar{D}^0$ cross sections for 150 energy points between 3.8 and 4.95 GeV. Here \sqrt{s} denotes the center of mass energy, \mathcal{L} is the integrated luminosity, $1+\delta$ is the ISR correction factor, $\frac{1}{|1-\Pi|^2}$ is the VP correction factor, ϵ is the detection efficiency, N_{obs} denotes the number of the observed signal events and σ^B represents the Born order cross section.

\sqrt{s} (GeV)	\mathcal{L} (pb $^{-1}$)	$(1+\delta)$	$\frac{1}{ 1-\Pi ^2}$	ϵ	N_{obs}	σ^B (pb)
3.80765	50.54	0.86	1.06	0.58	0.3 \pm 36.2	0.1 \pm 7.5 \pm 0
3.85000	7.967	1.12	1.05	0.49	181.4 \pm 16.7	219 \pm 20.1 \pm 14.2
3.89000	7.758	0.88	1.05	0.48	273.6 \pm 18.6	445.1 \pm 30.3 \pm 28.9
3.89500	7.567	0.88	1.05	0.49	262.5 \pm 19.1	432.2 \pm 31.5 \pm 28.1
3.89624	52.61	0.88	1.05	0.5	1801.7 \pm 49	415.2 \pm 11.3 \pm 27
3.90000	7.575	0.88	1.05	0.49	247.7 \pm 18.6	402.9 \pm 30.3 \pm 26.2
3.90500	7.596	0.88	1.05	0.5	249.5 \pm 28.5	398.8 \pm 45.6 \pm 25.9
3.91000	7.24	0.89	1.05	0.5	259.7 \pm 18.9	434 \pm 31.6 \pm 28.2
3.91500	7.454	0.9	1.05	0.5	261.2 \pm 19.1	416.1 \pm 30.4 \pm 27
3.92000	6.806	0.9	1.05	0.5	227.7 \pm 18.3	395.6 \pm 31.8 \pm 25.7
3.92500	6.694	0.92	1.05	0.5	192.8 \pm 17.3	334.8 \pm 30 \pm 21.8
3.93000	6.735	0.93	1.05	0.5	173.8 \pm 16.2	296.1 \pm 27.6 \pm 19.2
3.93500	7.161	0.94	1.05	0.5	197 \pm 18	311 \pm 28.4 \pm 20.2
3.94000	7.228	0.96	1.05	0.5	164.6 \pm 16.3	254.4 \pm 25.2 \pm 16.5
3.94500	7.59	0.98	1.05	0.49	207.8 \pm 18.8	301.3 \pm 27.2 \pm 19.6
3.95000	7.714	1	1.05	0.49	197 \pm 18.1	279.1 \pm 25.6 \pm 18.1
3.95500	8.124	1.03	1.05	0.48	157.3 \pm 17	206.1 \pm 22.2 \pm 13.4
3.96000	8.489	1.07	1.05	0.48	163.1 \pm 17.8	201.8 \pm 22 \pm 13.1
3.96500	7.768	1.11	1.05	0.47	149.2 \pm 16.9	197.3 \pm 22.3 \pm 12.8

3.97000	7.321	1.15	1.05	0.46	122.5 ± 15.2	169.2 ± 21 ± 11
3.97500	8.062	1.22	1.05	0.44	131.5 ± 19.7	160.2 ± 24.1 ± 10.4
3.98000	6.486	1.3	1.05	0.43	88.6 ± 15.3	131.3 ± 22.7 ± 8.5
3.98500	7.969	1.41	1.05	0.41	106.3 ± 15.7	123.3 ± 18.2 ± 8
3.99000	8.024	1.54	1.05	0.39	93.2 ± 15.6	102.9 ± 17.2 ± 6.7
3.99500	7.985	1.69	1.05	0.37	85.4 ± 16.2	91.6 ± 17.4 ± 6
4.00000	7.732	1.84	1.05	0.34	94.1 ± 17.9	102.2 ± 19.5 ± 6.6
4.00500	7.537	1.89	1.04	0.33	45.4 ± 12.8	52.4 ± 14.8 ± 3.4
4.00762	482	1.85	1.04	0.33	2710.6 ± 119.2	50.4 ± 2.2 ± 3.3
4.01000	7.183	1.76	1.04	0.33	62.2 ± 18.4	79.9 ± 23.6 ± 5.2
4.01200	6.907	1.67	1.04	0.33	33.5 ± 10.9	47.3 ± 15.4 ± 3.1
4.01400	6.694	1.56	1.04	0.34	14.7 ± 9.2	22.6 ± 14.1 ± 1.5
4.01600	6.544	1.45	1.04	0.35	21.6 ± 9.3	34.9 ± 15 ± 2.3
4.01800	6.968	1.35	1.04	0.36	70.2 ± 16.9	111.5 ± 26.8 ± 7.2
4.02000	6.726	1.26	1.04	0.37	39 ± 10.2	66.7 ± 17.4 ± 4.3
4.02500	6.538	1.07	1.05	0.41	94.1 ± 13.1	174.8 ± 24.3 ± 11.4
4.03000	16.451	0.95	1.05	0.44	381.4 ± 24.2	295.7 ± 18.7 ± 19.2
4.03500	6.706	0.88	1.05	0.46	184.6 ± 16.6	357 ± 32 ± 23.2
4.04000	6.564	0.84	1.05	0.48	195.9 ± 17.9	389.1 ± 35.5 ± 25.3
4.05000	6.567	0.82	1.05	0.51	230 ± 17.7	449.8 ± 34.6 ± 29.2
4.05500	6.927	0.81	1.05	0.51	201.4 ± 17.8	373.8 ± 33 ± 24.3
4.06000	6.338	0.82	1.05	0.52	221 ± 17.1	438.9 ± 33.9 ± 28.5
4.06500	7.022	0.83	1.05	0.52	200.3 ± 17.1	353.5 ± 30.2 ± 23
4.07000	7.271	0.84	1.05	0.52	242.1 ± 20.2	407.5 ± 34 ± 26.5
4.08000	7.721	0.86	1.05	0.52	279.2 ± 20.3	432.7 ± 31.4 ± 28.1
4.08545	52.86	0.87	1.05	0.53	1741.7 ± 50.5	382.9 ± 11.1 ± 24.9
4.09000	7.611	0.88	1.05	0.52	360.1 ± 23.1	544.9 ± 34.9 ± 35.4
4.10000	7.254	0.91	1.05	0.52	278.4 ± 20.2	435.5 ± 31.5 ± 28.3
4.11000	7.146	0.93	1.05	0.51	237.2 ± 19	368.8 ± 29.6 ± 24
4.12000	7.648	0.96	1.05	0.51	240.2 ± 19.8	341.7 ± 28.2 ± 22.2
4.12878	401.5	0.78	1.05	0.57	9239.5 ± 130.7	274.1 ± 3.9 ± 17.8
4.13000	7.207	0.98	1.05	0.5	204.2 ± 19.2	309.2 ± 29 ± 20.1
4.14000	7.268	1.01	1.05	0.48	164.8 ± 17.4	246.8 ± 26.1 ± 16
4.14500	7.774	1.02	1.05	0.49	209.9 ± 19.6	289.8 ± 27 ± 18.8
4.15000	7.662	1.04	1.05	0.48	141.3 ± 15.8	198.5 ± 22.3 ± 12.9
4.15783	408.7	0.84	1.05	0.57	6790.7 ± 113.8	183.5 ± 3.1 ± 11.9
4.16000	7.954	1.06	1.05	0.47	118.4 ± 23.7	160 ± 32 ± 10.4
4.17000	18.008	1.08	1.05	0.46	326 ± 24.7	194.9 ± 14.8 ± 12.7
4.18000	7.309	1.07	1.05	0.45	120.8 ± 14.3	181.9 ± 21.6 ± 11.8
4.18859	43.33	1.05	1.06	0.46	691.4 ± 35.1	173.7 ± 8.8 ± 11.3
4.18912	526.7	1.04	1.06	0.45	8949.4 ± 129.9	190.9 ± 2.8 ± 12.4
4.19000	7.56	1.04	1.06	0.45	102.8 ± 13.7	153.4 ± 20.5 ± 10
4.19500	7.503	1.02	1.06	0.45	123.2 ± 14.6	187.4 ± 22.2 ± 12.2
4.19915	526	1.01	1.06	0.45	9323.9 ± 130.6	204 ± 2.9 ± 13.3
4.20000	7.582	1.01	1.06	0.46	155.6 ± 15.8	234.9 ± 23.8 ± 15.3
4.20300	4.734	1.01	1.06	0.46	80.8 ± 12	194.7 ± 29 ± 12.7
4.20600	7.638	1.01	1.06	0.46	151.2 ± 15.3	226.6 ± 23 ± 14.7
4.20773	54.95	1.02	1.06	0.46	982.5 ± 41.3	200.4 ± 8.4 ± 13
4.20939	517.1	1.02	1.06	0.45	8260.7 ± 122.5	183.7 ± 2.7 ± 11.9
4.21000	7.678	1.02	1.06	0.45	142.5 ± 15.4	212.6 ± 22.9 ± 13.8
4.21500	7.768	1.05	1.06	0.45	144.9 ± 17.7	208.6 ± 25.5 ± 13.6
4.21713	54.6	1.07	1.06	0.45	796.7 ± 38.5	159.5 ± 7.7 ± 10.4
4.21893	514.6	1.08	1.06	0.44	7296.3 ± 119.4	158.5 ± 2.6 ± 10.3
4.22000	7.935	1.1	1.06	0.44	127.5 ± 14.5	175.7 ± 20 ± 11.4
4.22500	8.212	1.16	1.06	0.43	138.3 ± 15.8	178.9 ± 20.5 ± 11.6
4.22626	1100.94	1.18	1.06	0.43	13295.8 ± 164.3	124.3 ± 1.5 ± 8.1
4.23000	8.193	1.23	1.06	0.42	101.5 ± 13.7	127.4 ± 17.2 ± 8.3
4.23500	8.273	1.3	1.06	0.41	87.7 ± 14.1	106.4 ± 17.1 ± 6.9
4.23577	530.3	1.31	1.06	0.4	5096.1 ± 108.4	96 ± 2 ± 6.2
4.24000	7.83	1.34	1.06	0.39	69 ± 12.9	89.8 ± 16.8 ± 5.8
4.24166	55.88	1.34	1.06	0.4	528.6 ± 35.5	92.7 ± 6.2 ± 6
4.24300	8.571	1.35	1.06	0.38	69.5 ± 12.5	85.5 ± 15.4 ± 5.6
4.24397	538.1	1.35	1.06	0.38	4904.6 ± 111.2	92.6 ± 2.1 ± 6
4.24500	8.487	1.35	1.06	0.38	82.7 ± 12.9	98.9 ± 15.4 ± 6.4

4.24800	8.554	1.35	1.06	0.39	65.3 ± 14.7	76.7 ± 17.3 ± 5
4.25000	8.596	1.35	1.05	0.38	62.3 ± 11.5	74.5 ± 13.8 ± 4.8
4.25500	8.657	1.24	1.05	0.4	84.2 ± 12.2	103.8 ± 15 ± 6.7
4.25797	828.4	1.14	1.05	0.42	5839.8 ± 115.3	78.4 ± 1.5 ± 5.1
4.26000	8.88	1.29	1.05	0.4	80.8 ± 12.2	94.3 ± 14.2 ± 6.1
4.26500	8.629	1.35	1.05	0.38	70.4 ± 13.6	84.6 ± 16.4 ± 5.5
4.26681	531.1	1.35	1.05	0.38	4057.7 ± 100.4	80 ± 2 ± 5.2
4.27000	7.522	1.35	1.05	0.37	59.2 ± 11.1	82.7 ± 15.5 ± 5.4
4.27500	8.567	1.35	1.05	0.37	78.2 ± 12.2	97.7 ± 15.2 ± 6.4
4.27778	175.7	1.36	1.05	0.36	1205.5 ± 56.4	74.6 ± 3.5 ± 4.9
4.28000	8.723	1.36	1.05	0.37	39.3 ± 11.4	48.2 ± 13.9 ± 3.1
4.28500	8.596	1.36	1.05	0.36	62.9 ± 13.3	80.1 ± 17 ± 5.2
4.28843	502.4	1.04	1.05	0.47	3156.9 ± 93.2	68.5 ± 2 ± 4.5
4.29000	9.01	1.37	1.05	0.36	70.3 ± 14.7	84.8 ± 17.8 ± 5.5
4.30000	8.453	1.39	1.05	0.35	59.9 ± 12.6	78.4 ± 16.4 ± 5.1
4.30789	45.08	1.39	1.05	0.36	283.6 ± 25.9	67.7 ± 6.2 ± 4.4
4.31000	8.599	1.4	1.05	0.35	80.5 ± 13.5	103.2 ± 17.3 ± 6.7
4.31268	501.2	1.05	1.05	0.45	2969.3 ± 85.3	65.9 ± 1.9 ± 4.3
4.32000	9.342	1.4	1.05	0.34	67.9 ± 16	80.8 ± 19 ± 5.3
4.33000	8.657	1.38	1.05	0.34	37.9 ± 8.7	50.1 ± 11.5 ± 3.3
4.33793	505	1.03	1.05	0.45	2826.2 ± 84.3	64.2 ± 1.9 ± 4.2
4.34000	8.7	1.34	1.05	0.35	52.4 ± 11.3	69 ± 14.8 ± 4.5
4.35000	8.542	1.28	1.05	0.36	34.7 ± 10.4	46.9 ± 14 ± 3
4.35826	543.9	1.22	1.05	0.37	3470.7 ± 88.5	74.2 ± 1.9 ± 4.8
4.36000	8.063	1.21	1.05	0.37	49.3 ± 11.6	72.2 ± 17 ± 4.7
4.37000	8.498	1.15	1.05	0.39	69.1 ± 12	98 ± 17 ± 6.4
4.37788	522.7	0.91	1.05	0.49	3993.9 ± 111.2	91.9 ± 2.6 ± 6
4.38000	8.158	1.1	1.05	0.4	77.7 ± 12.3	114.7 ± 18.1 ± 7.5
4.38740	55.57	1.07	1.05	0.42	461.2 ± 31	98.4 ± 6.6 ± 6.4
4.39000	7.46	1.07	1.05	0.42	53.9 ± 9.5	86.6 ± 15.2 ± 5.6
4.39500	7.43	1.06	1.05	0.42	58.4 ± 10.6	93.6 ± 17 ± 6.1
4.39683	507.8	0.89	1.05	0.49	4767.3 ± 93.5	113.9 ± 2.2 ± 7.4
4.40000	7.178	1.05	1.05	0.43	66.3 ± 10.4	109 ± 17 ± 7.1
4.41000	6.352	1.03	1.05	0.43	54.1 ± 9.6	102.1 ± 18.2 ± 6.6
4.41558	1090.7	1.02	1.05	0.44	11704 ± 144.8	126.2 ± 1.6 ± 8.2
4.42000	7.519	1.01	1.05	0.44	77.1 ± 11.2	121.6 ± 17.7 ± 7.9
4.42500	7.436	1.01	1.05	0.45	94.9 ± 13.6	150.9 ± 21.6 ± 9.8
4.43000	6.788	1.01	1.05	0.45	93.9 ± 12.7	164.2 ± 22.2 ± 10.7
4.43710	569.9	0.89	1.05	0.51	6228.8 ± 106.6	127.9 ± 2.2 ± 8.3
4.44000	7.638	1.02	1.05	0.45	79.6 ± 12.9	121.2 ± 19.6 ± 7.9
4.45000	7.677	1.04	1.05	0.44	76.6 ± 12.7	114.9 ± 19.1 ± 7.5
4.46000	8.724	1.07	1.05	0.44	99.2 ± 13	128.4 ± 16.9 ± 8.3
4.46706	111.09	1.08	1.05	0.44	962 ± 70.8	97.4 ± 7.2 ± 6.3
4.48000	8.167	1.11	1.05	0.43	83.2 ± 11	113.8 ± 15.1 ± 7.4
4.50000	7.997	1.15	1.05	0.42	65.2 ± 10.8	90.7 ± 15 ± 5.9
4.52000	8.674	1.19	1.05	0.4	52 ± 10.8	66.8 ± 13.9 ± 4.3
4.52714	112.12	1.2	1.05	0.39	768.7 ± 42.4	77.3 ± 4.3 ± 5
4.54000	9.335	1.23	1.05	0.39	61.8 ± 11.3	74.4 ± 13.6 ± 4.8
4.55000	8.765	1.25	1.05	0.38	41 ± 9.6	52.7 ± 12.3 ± 3.4
4.56000	8.259	1.27	1.05	0.37	44.8 ± 9.2	61.3 ± 12.6 ± 4
4.57000	8.39	1.3	1.05	0.36	36.3 ± 9.3	49 ± 12.6 ± 3.2
4.57450	48.93	1.31	1.05	0.36	147.3 ± 19.3	33.6 ± 4.4 ± 2.2
4.58000	8.545	1.32	1.05	0.36	51.6 ± 10.5	68.3 ± 13.9 ± 4.4
4.59000	8.162	1.36	1.05	0.35	39.1 ± 10	53.6 ± 13.7 ± 3.5
4.59953	586.9	1.38	1.05	0.35	2628.2 ± 93.8	49.3 ± 1.8 ± 3.2
4.61186	103.83	1.13	1.05	0.41	462.9 ± 35.4	50.8 ± 3.9 ± 3.3
4.62800	521.52	1.09	1.05	0.41	2242 ± 74.2	51.2 ± 1.7 ± 3.3
4.64091	552.41	1.04	1.05	0.42	2394.5 ± 74.5	52.5 ± 1.6 ± 3.4
4.66124	529.63	1.01	1.05	0.43	2219.3 ± 73.1	50.8 ± 1.7 ± 3.3
4.68192	1669.31	1.05	1.05	0.43	7359.3 ± 131.9	51.8 ± 0.9 ± 3.4
4.69882	536.45	1.04	1.05	0.43	2400.9 ± 73.2	53.1 ± 1.6 ± 3.5
4.73970	164.27	1.07	1.05	0.42	716 ± 42.3	51 ± 3 ± 3.3
4.75005	367.21	1.08	1.05	0.42	1482.1 ± 62	47.3 ± 2 ± 3.1
4.78054	512.78	1.09	1.06	0.41	1940.8 ± 73.1	44.7 ± 1.7 ± 2.9

4.84307	527.29	1.12	1.06	0.4	1413.6 ± 65.8	$32 \pm 1.5 \pm 2.1$
4.91802	208.11	1.15	1.06	0.38	608 ± 39.6	$35.1 \pm 2.3 \pm 2.3$
4.95093	160.37	1.16	1.06	0.37	435.3 ± 38.3	$33.2 \pm 2.9 \pm 2.2$

TABLE III: The $e^+e^- \rightarrow D^+D^-$ cross sections for 150 energy points between 3.8 and 4.95 GeV. Here \sqrt{s} denotes the center of mass energy, \mathcal{L} is the integrated luminosity, $1+\delta$ is the ISR correction factor, $\frac{1}{|1-\Pi|^2}$ is the VP correction factor, ϵ is the detection efficiency, N_{obs} denotes the number of the observed signal events and σ^B represents the Born order cross section.